Electric Power Systems Research 249 (2025) 112004

Contents lists available at ScienceDirect

Electric Power Systems Research

journal homepage: www.elsevier.com/locate/epsr

Direct data-driven control of grid-connected DERs using Taylor series expansion☆

Zhongtian Zhang [a], Javad Khazaei [a,*], Faegheh Moazeni [b], Pietro Tesi [c], Claudio De Persis [d]

[a] Department of Electrical and Computer Engineering, Lehigh University, Bethlehem, 18015, PA, USA
[b] Department of Civil and Environmental Engineering, Lehigh University, Bethlehem, 18015, PA, USA
[c] University of Florence, Florence, 50139, Italy
[d] University of Groningen, Groningen, Netherlands

ARTICLE INFO

Keywords:
Distributed energy resources
Control systems
Data-driven control
Taylor series expansion

ABSTRACT

Incorporation of distributed energy resources (DERs) - including a range of renewable energy technologies and energy storage solutions into the power grid can provide cost savings, reduce CO_2 emissions, and enhance the resilience of the grid. However, traditional approaches for the control of DERs rely heavily on pre-established models and systems identification tools, which are often difficult to obtain and might not be able to capture parameter changes or uncertainties. This paper proposes a new direct control design for primary control of grid-connected DERs using Taylor series expansion and Lyapunov's linearization method. Utilizing available DER data, the control design of nonlinear DERs is converted to a data-centered convex optimization program, which guarantees stability and robustness against noise. Compared with existing model-free control designs that heavily rely on machine learning methods, require a large amount of data, and cannot provide stability guarantees, the proposed method requires minimum data, is generalizable to various DER operating conditions, and provides stability guarantees. Time-domain simulations on detailed DER models with power electronics switching details validate the effectiveness of the proposed data-centered DER control approach.

1. Introduction

Distributed energy resources (DER), such as renewables and storage, are critical to meeting the net zero emissions target of 2050, but their improper control can destabilize the power grid and lead to outages. For example, in 2020, the loss of more than 1000 MW of power from a solar DER in southern California after a grid fault was attributed to the DER controllers [1].

Since DER control objectives vary in real time, the DER control requires a hierarchical structure that includes primary, secondary, and tertiary control. Techniques for primary control of DERs can be classified as model-based or model-free, depending on whether the control relies on a DER model. Model-based techniques include both linear control strategies [2] and nonlinear ones [3]. By linearizing the DER model around an operating point, classical vector control strategies use linear regulators for hierarchical control [2]. For nonlinear DER controllers, several approaches have been proposed, including Lyapunov theory and feedback linearization [3], backstepping [4], and sliding mode control [5]. Model-based techniques can derive a system model from first-principle laws or from data, with the latter approach termed data-driven of *indirect* type, as controller design involves an intermediate identification step. In contrast to model-based techniques, model-free techniques, which are also called data-driven techniques of *direct* type, do not explicitly rely on a model of the system. Instead, they design the control law directly via optimization methods applied to datasets collected from the system. Direct approaches that have been proposed for DER control include neural networks [6], model-free adaptive control [7], model-free predictive control [8], and reinforcement learning [9].

Direct methods have some potential advantages. They do not rely on a model of the system, which can be challenging to derive, especially

☆ This research was in part under support from the National Science Foundation, United States under Grant NSF-EPCN 2221784. Javad Khazaei, Faegheh Moazeni and Zhongtian Zhang are with the college of Engineering at Lehigh University, Bethlehem, PA 18015 USA, Pietro Tesi is with the department of Information Engineering at Università Degli Studi Firenze (University of Florence), Italy, Claudio De Persis is with the faculty of Science and Engineering at University of Groningen, Netherlands.

* Corresponding author.
E-mail addresses: zhz819@lehigh.edu (Z. Zhang), jak921@lehigh.edu (J. Khazaei), fam321@lehigh.edu (F. Moazeni), pietro.tesi@nifi.it (P. Tesi), c.de.persis@rug.nl (C. De Persis).

https://doi.org/10.1016/j.epsr.2025.112004
Received 11 April 2025; Received in revised form 26 June 2025; Accepted 7 July 2025
Available online 21 July 2025

in the case of DERs that feature complex nonlinear dynamics [10,11]. Model-based design can also be computationally demanding and lack robustness [12,13]. Another potential advantage of direct techniques is that identification can produce models that are not suitable for control design because control objectives are not explicitly taken into account during the identification phase [14,15]. However, direct techniques currently have some significant limitations. These include limited performance (due to the large number of samples usually required for good performance), lack of interpretability (due to the absence of a physical model, making it difficult to understand the controller policy or debug control issues), and difficulty in generalizing to unseen situations [16,17].

Driven by the challenges mentioned above, this paper aims to introduce a model-free methodology that diverges from current learning-based techniques. Building on existing work in [18,19], our proposed approach focuses on reducing the dependency on large data sets, prioritizing interpretability, and ensuring stability and robustness. Specifically, our goal is to recreate the *Lyapunov's linearization* method using data as a non-parametric system model. Consequently, we develop a robust controller for the linearized dynamics around the desired equilibrium point, treating the high-order nonlinearities (represented by the remainder term of the Taylor expansion) as uncertainty. With this approach, it becomes sufficient to know the order of magnitude of the nonlinearities rather than their analytical expression. We demonstrate the effectiveness of this approach, since the design leads to computationally efficient convex optimization problems. Since Lyapunov design is not restricted to special classes of systems, we thus provide a data-centric approach to controller design that is computationally efficient and ensures broad applicability.

The specific contributions of this paper are as follows.

(i) Utilizing available DER data to provide a non-parametric representation of the closed-loop nonlinear dynamics, which is turned into a convex controller design program using Lyapunov's linearization method;
(ii) A direct design for primary control of DERs (current and active/reactive powers) with stability guarantees and robustness against noise without requiring an explicit DER model;
(iii) Real-time simulations and validation of proposed control design on a detailed DER model with power electronics switching for active/reactive power tracking, robustness against noise, and detailed comparison with conventional vector controllers.

The remainder of the paper is organized as follows. Section 2 presents the problem formulation, the DER modeling, and the control architecture. Section 3 describes the proposed control design approach and provides main results and discussion. Section 4 reports real-time simulations on a case study, and Section 5 ends the paper with concluding remarks and open research questions for future work.

2. Problem formulation

A DER is depicted in Fig. 1 with its power electronics interface (converter) and filtering component (RLC filter), which is connected to the main electricity grid at the point of common coupling (PCC). The power converter is mainly composed of a voltage source DC/AC converter fed by the energy resource (solar, wind, or battery) through a DC link. Each DER unit can be controlled as an AC voltage source through an adjustable voltage magnitude and angle in the PCC, $v_s e^{j\omega_s t}$ [20]. This is achieved through inner current regulators, as explained in [21]. Therefore, the variables v_s and ω_s determine the forced response of the DER unit and therefore are considered as input variables of the dynamic model. Similarly, the rest of the grid can also be assumed to behave as an AC voltage source modeled as a lumped AC voltage source $v_g e^{j\omega_g t}$ with a series impedance [20]. In the grid-connected mode, v_g and ω_g can be assumed to have fixed values, but in the off-grid mode, these are dynamic variables. The lumped model presented in [20] was shown to accurately capture the transient interaction between the DER and the rest of the grid and, therefore, it was adopted in our study.

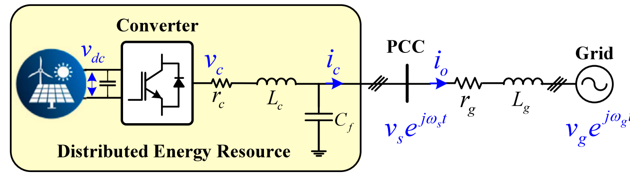

Fig. 1. A DER connected to the grid.

2.1. Lumped dynamical model of DERs

The lumped model depicted in Fig. 1 can be described by a set of differential equations assuming that a synchronous reference frame aligns with v_s [20]:

$$\begin{cases} L_g \dfrac{d\boldsymbol{i}_o}{dt} &= -r_g \boldsymbol{i}_o - j\omega_s L_g \boldsymbol{i}_o - v_g e^{j\delta} + v_s \\ \dfrac{d\delta}{dt} &= \omega_g - \omega_s \end{cases} \tag{1}$$

where r_c, L_c, C_f are the filter components of the converter, r_g and L_g are the grid impedance components, v_s is the converter voltage in the PCC, v_g is the grid voltage, i_c is the converter current, and i_o is the output current. By decomposing Eq. (1) into the real and imaginary parts, we can write the model in state-space form corresponding to a control-affine nonlinear system:

$$\dot{\mathbf{x}} = \mathbf{f}(\mathbf{x}) + \mathbf{g}(\mathbf{x})\mathbf{u}, \tag{2}$$

where

$$\mathbf{f}(\mathbf{x}) = \begin{bmatrix} -\dfrac{r_g}{L_g}x_1 - \dfrac{v_g}{L_g}\cos x_3 \\ -\dfrac{r_g}{L_g}x_2 - \dfrac{v_g}{L_g}\sin x_3 \\ \omega_g \end{bmatrix}, \quad \mathbf{g}(\mathbf{x}) = \begin{bmatrix} \dfrac{1}{L_g} & x_2 \\ 0 & -x_1 \\ 0 & -1 \end{bmatrix}. \tag{3}$$

(In this paper, v_i denotes the ith component of the vector $\mathbf{v}$.) In Eq. (3), $\mathbf{x} = [i_{od}\ i_{oq}\ \delta]^\top$ represents the state vector while $\mathbf{u} = [v_s\ \omega_s]^\top$ is the input vector of the DER unit, which includes the amplitude and voltage angle at the PCC. It is noted that the angle δ is a state variable of the model. As discussed in [20], it might be difficult to measure directly δ. In this case, the control design must be carried out based on a subset of state variables, namely $\mathbf{y} = [i_{od}\ i_{oq}]^\top$. Throughout this paper, for the sake of simplicity, we assume that the whole state $\mathbf{x}$ is available for measurements. An extension of the ideas discussed in this paper to partial state information and input–output data has recently been presented in [22].

2.2. Control objective

The control objective is to design a control law $u = \mathcal{K}(x)$ that stabilizes the system around an equilibrium point $(\mathbf{x_e}, \mathbf{u_e})$ of interest. Given $\mathbf{x} = [i_{od}\ i_{oq}\ \delta]^\top$, the operating region for the system is defined as $\underline{\mathbf{x}} \le \mathbf{x} \le \bar{\mathbf{x}}$, where $\underline{\mathbf{x}}$ is the minimum operating point and $\bar{\mathbf{x}}$ is the maximum operating point, both of which to be decided based on the capacity of the DER. (Here, the constraints are understood to hold element-wise.) For example, for a DER with nominal power of $P = 10$ kW connected to a $V_\phi = 400$ V grid (line to neutral), following the relationship $P = 3V_\phi I_\phi \cos\theta$, the maximum current of the DER at a unity power factor (that is, $\theta = 0$) will be $\bar{I}_\phi = 25$ A, which decides the maximum $\bar{i}_{od}, \bar{i}_{oq}$ following the relationship $\bar{I}_\phi^2 = \bar{i}_{od}^2 + \bar{i}_{oq}^2$.

By enforcing the steady-state condition $0 = f(\mathbf{x_e}) + g(\mathbf{x_e})\mathbf{u_e}$, we obtain the equilibrium points of the system as solutions to a set of algebraic nonlinear equations.

$$\begin{bmatrix} -\dfrac{r_g}{L_g}x_{e1} - \dfrac{v_g}{L_g}\cos(x_{e3}) \\ -\dfrac{r_g}{L_g}x_{e2} - \dfrac{v_g}{L_g}\sin(x_{e3}) \\ \omega_g \end{bmatrix} = \begin{bmatrix} -\dfrac{u_{e1}}{L_g} - x_{e2}u_{e2} \\ x_{e1}u_{e2} \\ u_{e2} \end{bmatrix}. \tag{4}$$

We can choose an equilibrium point using a fixed value of $x_1 = i_{od}$ and $x_2 = i_{oq}$ to define the other equilibrium conditions. For example, if the reference inputs for active and reactive power control (P^{ref}, Q^{ref}) of the DER connected to the grid are known from the automatic generation control (AGC), the setpoints of the currents can be found, namely i_{od}^{ref} and i_{oq}^{ref} through active and reactive power injections at the PCC. In that case, given that $\delta \approx 0$ in the steady-state due to the incorporation of a phase-locked loop (PLL) that synchronizes the converter with the grid at the PCC, we can write $v_s = |v_s|\angle\delta = v_{sd} + jv_{sq} \approx v_{sd}$ and find the setpoints of the currents as

$$i_{od}^{ref} = \frac{P^{ref}}{1.5v_s}, \quad i_{oq}^{ref} = -\frac{Q^{ref}}{1.5v_s}. \tag{5}$$

As a result, in the steady state, the current tracking error will be zero and thus $x_{e1} = i_{od}^{ref}$ and $x_{e2} = i_{og}^{ref}$. Having x_{e1} and using the third equation in (4), one can write $u_{e2} = \omega_g$. Next, x_{e3} and u_{e1} can be found from the second and first equations in (4), respectively:

$$x_{e3} = \arcsin\left(-\frac{r_g}{v_g}x_{e2} - \frac{L_g}{v_g}x_{e1}u_{e2}\right), \tag{6}$$

$$u_{e1} = r_g x_{e1} + v_g\cos(x_{e3}) - L_g x_{e2}u_{e2}. \tag{7}$$

For model-based methods, including indirect data-driven methods, equilibria can be calculated based on the model. In direct data-driven methods, as we will consider in Section 3, determining the equilibria requires domain knowledge. In this regard, it is worth noting that knowledge of the equilibria can also be extracted from any existing control system. In fact, the equilibrium condition is *controller-independent* as it is uniquely determined by the relationship $0 = f(\mathbf{x_e}) + g(\mathbf{x_e})\mathbf{u_e}$. This means that the equilibrium points can be inferred from any system in steady-state regime, including those empirically determined (e.g., classic PID tuning) or preliminarily obtained with poorly performing controllers.

2.3. Stabilization via Taylor's expansion

The Lyapunov linearization method is one of the most popular approaches to controller design for nonlinear systems [23]. Consider the system $\dot{\mathbf{x}} = f(\mathbf{x}) + g(\mathbf{x})\mathbf{u}$ with equilibrium $(\mathbf{x_e}, \mathbf{u_e})$. The first-order Taylor's expansion of the vector field around the equilibrium is given by $f(\mathbf{x}) + g(\mathbf{x})\mathbf{u} = A\tilde{\mathbf{x}} + +B\tilde{\mathbf{u}} + r(\tilde{\mathbf{x}}, \tilde{\mathbf{u}})$ where $\tilde{\mathbf{x}} := \mathbf{x} - \mathbf{x_e}$ and $\tilde{\mathbf{u}} := \mathbf{u} - \mathbf{u_e}$ are the new state and input variables,

$$A := \left.\frac{\partial(f(\mathbf{x}) + g(\mathbf{x})\mathbf{u})}{\partial\mathbf{x}}\right|_{(\mathbf{x},\mathbf{u})=(\mathbf{x_e},\mathbf{u_e})}, \tag{8}$$

$$B := \left.\frac{\partial(f(\mathbf{x}) + g(\mathbf{x})\mathbf{u})}{\partial\mathbf{u}}\right|_{(\mathbf{x},\mathbf{u})=(\mathbf{x_e},\mathbf{u_e})}, \tag{9}$$

and $r(\tilde{\mathbf{x}}, \tilde{\mathbf{u}})$ is the so-called *remainder*, which is a function that converges to zero faster than linearly:

$$\lim_{(\tilde{\mathbf{x}},\tilde{\mathbf{u}})\to 0} \frac{|r(\tilde{\mathbf{x}}, \tilde{\mathbf{u}})|}{|(\tilde{\mathbf{x}}, \tilde{\mathbf{u}})|} = 0. \tag{10}$$

Consider now a feedback law $\tilde{\mathbf{u}} = K\tilde{\mathbf{x}}$ that makes $A + BK$ Hurwitz. (By Hurwitz, we mean that all eigenvalues have negative real parts.) It follows from Lyapunov's linearization method [23, Theorem 4.13] that this control law renders the origin an asymptotically stable equilibrium for the closed-loop dynamics $\dot{\tilde{\mathbf{x}}} = f(\tilde{\mathbf{x}}) + g(\tilde{\mathbf{x}})K\tilde{\mathbf{x}}$, therefore stabilizes the original system around $\mathbf{x_e}$. In the original coordinates, the control law takes the form of

$$\mathbf{u} = \mathbf{u_e} + K(\mathbf{x} - \mathbf{x_e}), \tag{11}$$

and the corresponding block diagram is shown in Fig. 2.

For completeness, we report the analytical expression of Taylor's expansion of a grid-connected DER relative to an arbitrary equilibrium

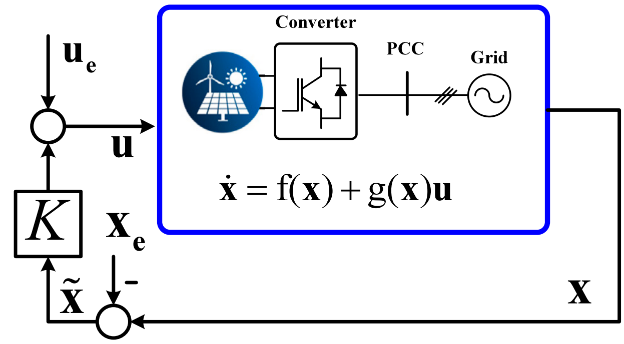

Fig. 2. Block diagram of the control architecture.

$(\mathbf{x_e}, \mathbf{u_e})$. Specifically, by writing (1) as $\dot{\tilde{\mathbf{x}}} = f(\tilde{\mathbf{x}} + \mathbf{x_e}) + g(\tilde{\mathbf{x}} + \mathbf{x_e})(\tilde{\mathbf{u}} + \mathbf{u_e})$ and rearranging the terms, we obtain $\dot{\tilde{\mathbf{x}}} = \tilde{f}(\tilde{\mathbf{x}}) + \tilde{g}(\tilde{\mathbf{x}})\tilde{\mathbf{u}}$, where

$$\tilde{f}(\tilde{\mathbf{x}}) = \begin{bmatrix} \frac{v_g}{L_g}\left(\cos(x_{e3}) - \cos(\tilde{x}_3 + x_{e3})\right) - \frac{r_g}{L_g}\tilde{x}_1 + \tilde{x}_2 u_{e2} \\ \frac{v_g}{L_g}\left(\sin(x_{e3}) - \sin(\tilde{x}_3 + x_{e3})\right) - \frac{r_g}{L_g}\tilde{x}_2 - \tilde{x}_1 u_{e2} \\ 0 \end{bmatrix},$$
$$\tilde{g}(\tilde{\mathbf{x}}) = \begin{bmatrix} \frac{1}{L_g} & \tilde{x}_2 + x_{e2} \\ 0 & -\tilde{x}_1 - x_{e1} \\ 0 & -1 \end{bmatrix}. \tag{12}$$

Therefore, the state and input matrices of the linearized system are given by:

$$A = \begin{bmatrix} -\frac{r_g}{L_g} & u_{e2} & \frac{v_g}{L_g}\sin x_{e3} \\ -u_{e2} & -\frac{r_g}{L_g} & -\frac{v_g}{L_g}\cos x_{e3} \\ 0 & 0 & 0 \end{bmatrix}, \quad B = \begin{bmatrix} \frac{1}{L_g} & x_{e2} \\ 0 & -x_{e1} \\ 0 & -1 \end{bmatrix}. \tag{13}$$

and the remainder term is given by:

$$r(\tilde{\mathbf{x}}, \tilde{\mathbf{u}}) = \begin{bmatrix} \frac{v_g}{L_g}\left(\sin x_{3e}(\sin\tilde{x}_3 - \tilde{x}_3) + \cos x_{3e}(1 - \cos\tilde{x}_3)\right) + \tilde{x}_2\tilde{u}_2 \\ \frac{v_g}{L_g}\left(\sin x_{3e}(1 - \cos\tilde{x}_3) - \cos x_{3e}(\sin\tilde{x}_3 - \tilde{x}_3)\right) - \tilde{x}_1\tilde{u}_2 \\ 0 \end{bmatrix}. \tag{14}$$

We observe that the remainder indeed converges to zero faster than $(\tilde{\mathbf{x}}, \tilde{\mathbf{u}})$ according to (10).

3. Direct data-driven controller design

The standard approach to Lyapunov design is model-based. In fact, to have stability we must design K in such a way that $A+BK$ is Hurwitz and for that we need information about A, B. However, reconstructing exactly A, B (from first-principle laws or from data) might be difficult. An option is to build a *robust* controller around A and B, namely a controller K that renders $(A + \Delta A) + (B + \Delta B)K$ Hurwitz for all ΔA, ΔB that satisfy norm constraints of the type $\|\Delta A\| \le \epsilon$ and $\|\Delta B\| \le \epsilon$, where $\epsilon > 0$ is a design parameter [24]. In this way, we ensure that the controller design is robust against imprecise modeling or identification. An alternative is to design a controller *directly* from the data without an explicit identification step. In this section, we discuss this alternative design approach.

Consider again the system (3) with a data set of inputs, states and state derivatives $\{(\mathbf{u}(t_k), \mathbf{x}(t_k), \dot{\mathbf{x}}(t_k)), k = 1, 2, \ldots, T\}$ that satisfy $\dot{\mathbf{x}}(t_k) = \mathbf{f}(\mathbf{x}(t_k)) + \mathbf{g}(\mathbf{x}(t_k))\mathbf{u}(t_k)$, where the time instants t_k are the sampling instants and $T > 0$ is the number of samples. (We will comment later on the assumption that we can measure the state derivative.) Recall now that Taylor's expansion of the system around and equilibrium point $(\mathbf{x_e}, \mathbf{u_e})$ is given by $\dot{\tilde{\mathbf{x}}} = A\tilde{\mathbf{x}} + B\tilde{\mathbf{u}} + r(\tilde{\mathbf{x}}, \tilde{\mathbf{u}})$ where $\tilde{\mathbf{x}} := \mathbf{x} - \mathbf{x_e}$ and $\tilde{\mathbf{u}} := \mathbf{u} - \mathbf{u_e}$, and A, B are as in (13). Since $\dot{\tilde{\mathbf{x}}} = \dot{\mathbf{x}}$, we have the following data-based relationship:

$$\dot{\mathbf{x}}(t_k) = A\tilde{\mathbf{x}}(t_k) + B\tilde{\mathbf{u}}(t_k) + r(\tilde{\mathbf{x}}(t_k), \tilde{\mathbf{u}}(t_k)) \tag{15}$$

for all $k = 1, 2, \dots, T$.

For brevity, let $\mathbf{r}(t_k) := r(\tilde{\mathbf{x}}(t_k), \tilde{\mathbf{u}}(t_k))$ and introduce the data matrices.

$$\begin{aligned} \mathbf{X}_d &:= \begin{bmatrix}\dot{\mathbf{x}}(t_1) & \dot{\mathbf{x}}(t_2) & \dots & \dot{\mathbf{x}}(t_T)\end{bmatrix}, \\ \tilde{\mathbf{X}} &:= \begin{bmatrix}\tilde{\mathbf{x}}(t_1) & \tilde{\mathbf{x}}(t_2) & \dots & \tilde{\mathbf{x}}(t_T)\end{bmatrix}, \\ \tilde{\mathbf{U}} &:= \begin{bmatrix}\tilde{\mathbf{u}}(t_1) & \tilde{\mathbf{u}}(t_2) & \dots & \tilde{\mathbf{u}}(t_T)\end{bmatrix}, \\ \mathbf{R} &:= \begin{bmatrix}\mathbf{r}(t_1) & \mathbf{r}(t_2) & \dots & \mathbf{r}(t_T)\end{bmatrix}. \end{aligned} \tag{16}$$

The identity (15) can thus be written in compact form as

$$\mathbf{X}_d = A\tilde{\mathbf{X}} + B\tilde{\mathbf{U}} + \mathbf{R}. \tag{17}$$

We can use this relation to derive a data-based (model-free) representation of the *closed-loop* dynamics with the feedback law $\tilde{\mathbf{u}} = K\tilde{\mathbf{x}}$. Consider any $K \in \mathbb{R}^{m\times n}$ and suppose that we can solve with respect to $G \in \mathbb{R}^{T\times n}$ the following system of equations (*cf.* Section 3.A):

$$\begin{bmatrix} I_n \\ K \end{bmatrix} = \begin{bmatrix} \tilde{\mathbf{X}} \\ \tilde{\mathbf{U}} \end{bmatrix} G. \tag{18}$$

By pre-multiplying both sides by $\begin{bmatrix}A & B\end{bmatrix}$ and exploiting (17) we obtain $A + BK = (\mathbf{X}_d - \mathbf{R})G$. Therefore, the closed-loop dynamics with $\tilde{\mathbf{u}} = K\tilde{\mathbf{x}}$ can be expressed as follows:

$$\dot{\tilde{\mathbf{x}}} = (\mathbf{X}_d - \mathbf{R})G\tilde{\mathbf{x}} + r(\tilde{\mathbf{x}}, \tilde{\mathbf{u}}). \tag{19}$$

In essence, this tells us that we can obtain an *equivalent* representation of closed-loop dynamics in which A, B are replaced by data and G is a *proxy* for K. We can thus ensure closed-loop stability by designing G such that $I_n = \tilde{\mathbf{X}}G$ and $(\mathbf{X}_d - \mathbf{R})G$ is Hurwitz, and then setting $K = \tilde{\mathbf{U}}G$. This gives a design procedure that can be carried out *without knowing exactly* to carry out the dynamics of the system, either A, B or the remainder term $r(\tilde{\mathbf{x}}, \tilde{\mathbf{u}})$. As shown next, we only need to know the bound on $\mathbf{R}$, which is a much less stringent requirement than the exact identification of the whole dynamics. Specifically, since $\mathbf{R}$ is unknown, we search for a matrix G that renders $(\mathbf{X}_d - R)G$ Hurwitz *for all* the matrices R that belong to a set $\mathcal{R}$ that is deemed to contain $\mathbf{R}$. Formally, define $\mathcal{R} := \{R \in \mathbb{R}^{n\times T} : RR^\top \preceq \Delta_R\Delta_R^\top\}$ where $\Delta_R \in \mathbb{R}^{n\times s}$ is a design parameter. We have the following result.

Theorem 1. *Consider system (3) along with an equilibrium* $(\mathbf{x_e}, \mathbf{u_e})$. *Consider the following program in the decision variables* $P \succ 0, \lambda > 0, Y$:

$$\begin{cases} \text{minimize} \quad 0 \\ \text{subject to} \\ \quad \begin{bmatrix} \mathbf{X}_d Y + (\mathbf{X}_d Y)^\top + \lambda\Delta_R\Delta_R^\top + \Omega & Y^\top \\ Y & -\lambda I_T \end{bmatrix} \preceq 0 \\ \quad P = \tilde{\mathbf{X}}Y \end{cases} \tag{20}$$

where $\Omega \succ 0$ *is chosen arbitrarily. If* $\mathbf{R} \in \mathcal{R}$ *and the program is feasible, then the control law* $\mathbf{u} = \mathbf{u_e} + K(\mathbf{x} - \mathbf{x_e})$ *with* $K = \tilde{\mathbf{U}}YP^{-1}$ *makes the equilibrium asymptotically stable for closed-loop dynamics.*

Proof. By Schur complement, the linear matrix inequality appearing in (20) is equivalent to:

$$\mathbf{X}_d Y + (\mathbf{X}_d Y)^\top + \lambda\Delta_R\Delta_R^\top + \lambda^{-1}Y^\top Y + \Omega \preceq 0. \tag{21}$$

Since $\mathbf{R} \in \mathcal{R}$ we further have

$$\mathbf{X}_d Y + (\mathbf{X}_d Y)^\top + \lambda\mathbf{R}\mathbf{R}^\top + \lambda^{-1}Y^\top Y + \Omega \preceq 0. \tag{22}$$

A completion of squares gives $-\mathbf{R}Y - (\mathbf{R}Y)^\top \preceq \lambda\mathbf{R}\mathbf{R}^\top + \lambda^{-1}Y^\top Y$ for all $\lambda > 0$. (This is known as *Young's inequality*.) In turn, this gives

$$(\mathbf{X}_d - \mathbf{R})Y + Y^\top(\mathbf{X}_d - \mathbf{R})^\top + \Omega \preceq 0. \tag{23}$$

Finally, let $G := YP^{-1}$ and observe that the two constraints $P = \tilde{\mathbf{X}}Y$ and $K = \tilde{\mathbf{U}}YP^{-1}$ are equivalent to (18). This implies $(\mathbf{X}_d - \mathbf{R})G = A + BK$. Thus, multiplying (23) left and right by P^{-1} gives

$$P^{-1}(A + BK) + (A + BK)^\top P^{-1} + P^{-1}\Omega P^{-1} \preceq 0. \tag{24}$$

This is the Lyapunov condition for stability which implies that $A + BK$ is Hurwitz. In turn, Lyapunov's theorem ensures that equilibrium $(\mathbf{x_e}, \mathbf{u_e})$ is asymptotically stable, and this concludes the proof. ■

The structure of the proposed controller and its integration into a DER is depicted in Fig. 3. As can be observed, the data are collected to solve the semi-definite program in (20) and find the controller gain K for the inner current regulator. In addition, the conventional phase-locked loop (PLL) must be modified to account for the converter voltage angle δ_0, as shown in the figure. The PLL compensator $G(s)$ is a proportional integral regulator, which is tuned to ensure the converter is synchronized to the grid and the voltage angle at the converter terminal is regulated to δ_0. Since v_q is no longer zero (due to the regulation of the converter voltage to δ_0, the active and reactive power control design should be achieved using two PI regulators with transfer functions $G_P(s)$ and $G_Q(s)$, respectively. To design PI regulators, one can utilize the bandwidth of the power controllers to be 10 times slower than the current regulator bandwidth.

3.1. Discussion

This method does not construct a model estimate, and for this reason it can be considered a *direct* method. However, we note that there is an identification process as data are used to infer the behavior of the system in closed loop. From a certain point of view, the difference with indirect methods is thus less pronounced than may appear at first glance. Identifying the behavior in the closed-loop still has some distinctive features. Firstly, the control design mechanism is very simple as it allows us to directly incorporate data into a stability criterion. Not only that, but the specific representation of the closed-loop system based on Taylor's series expansion is also advantageous. By virtue of this representation, we can treat the nonlinearity as an uncertainty term. As a result, in the spirit of robust control, we only need to know the order of magnitude of the nonlinearities (the uncertainty) and not their analytical expression.

We close this section by discussing some practical aspects of this method.

Estimation of the derivative matrix $\dot{\mathbf{X}}$*:* Differential equations can be solved numerically using a difference approximation. Taylor series expansions can be used to approximate the derivatives of a smooth function in the neighborhood of the point x. For smooth functions, the central difference approximation is more accurate. Therefore, following the central difference approximation concept, the $\dot{\mathbf{X}}$ can be obtained by:

$$\dot{\mathbf{X}} \approx \frac{\mathbf{X}(i+1) - \mathbf{X}(i-1)}{2h} \tag{25}$$

In the above formula, $\mathbf{X}(i)$ is the ith measurement vector and h is the sampling interval of the measurement system [25]. This approach was tested for distributed energy resources in our preliminary research [26].

Robustness to noise and computational aspects. The very same method can be used to account for noisy data [27] and/or inaccuracy in the computation of state derivatives [28]. In either case, we obtain an additional uncertainty term, say $\mathbf{S}$, which adds to that due to nonlinearities, resulting in a dynamics of the form $\mathbf{X}_d = A\tilde{\mathbf{X}} + B\tilde{\mathbf{U}} + \mathbf{R} + \mathbf{S}$, see [18]. The design program thus remains the same as long as we know an upper bound for this additional term. Another interesting aspect of this method is that the design program is structured as a semidefinite program and can thus be solved using standard tools for convex optimization such as CVX and YALMIP.

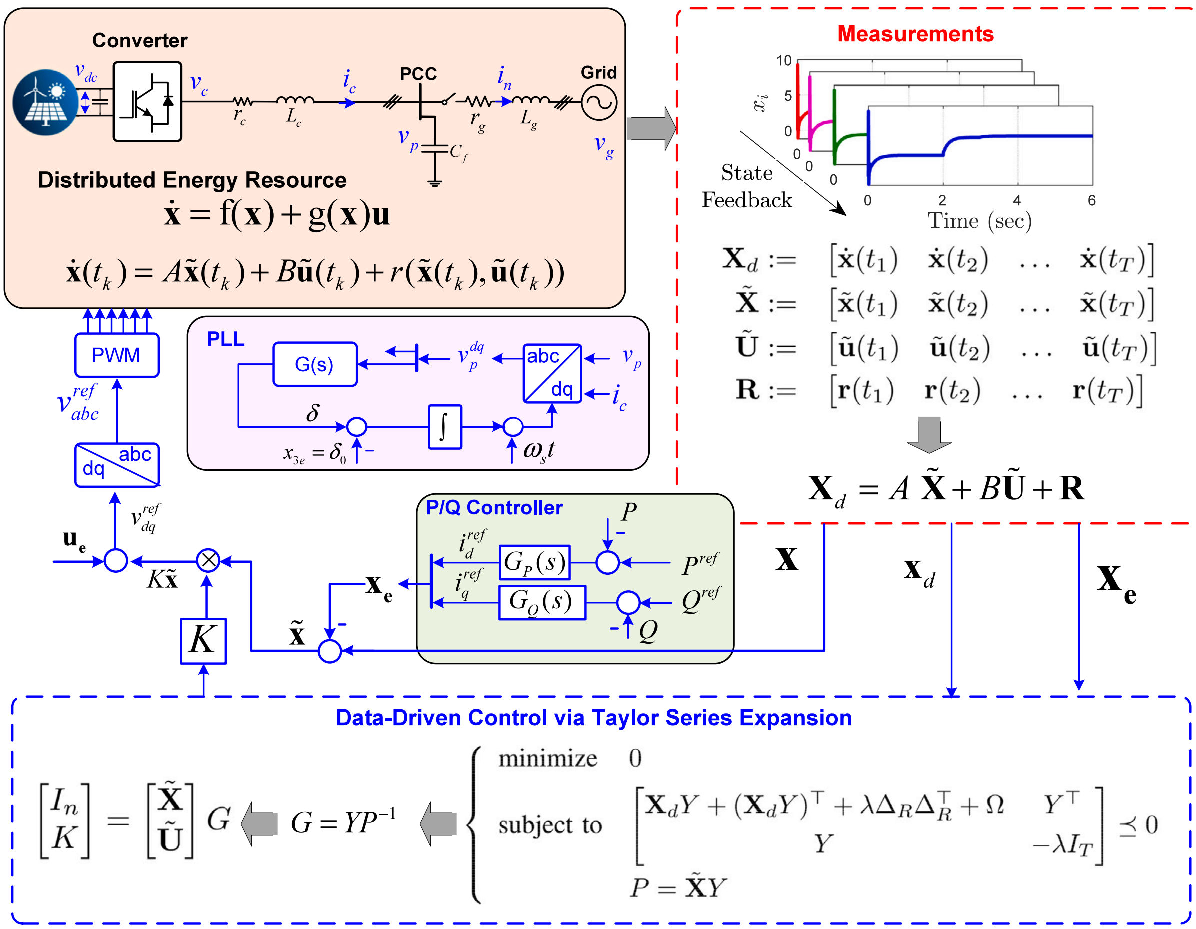

Fig. 3. Structure of the proposed data-driven DER control using Taylor series expansion.

Data quality and experiment design. Eq. (18) highlights, albeit implicitly, the importance of having a rich data set. In fact, if the matrix $[\begin{smallmatrix}\tilde{\mathbf{X}} \\ \tilde{\mathbf{U}}\end{smallmatrix}]$ has a full row rank, then (18) will have a solution for any controller K, meaning that no controller is excluded from the search. In contrast, when the data are not rich enough, only certain controllers may be admissible solutions, namely those in the image of $\tilde{\mathbf{U}}$. In the context of data-driven control, the problem of ensuring rich datasets for nonlinear systems has recently been discussed in [29]. It should be noted that the proposed design is not an online control design and is carried out in close to real-time, therefore, any missing data can be handled offline, for example, by collecting continuous sample data that do not include missing information. If a continuous-time sample $\tilde{\mathbf{X}} := [\tilde{\mathbf{x}}(t_1) \ \ \tilde{\mathbf{x}}(t_2) \ \ \dots \ \ \tilde{\mathbf{x}}(t_T)]$ is not available and information is missing during data collection, interpolation techniques can be used to recover missing information. Similarly, if the measurement includes noise with low signal-to-noise ratio (SNR), a priori filtering techniques such as Savitzky-Golay filtering, which we have explored in our preliminary research on sparse identification [30] can be utilized.

Incorporating prior knowledge. It is often the case that we know that some state variables do not include nonlinear terms (for example, a state variable describing the position-to-velocity relation). In such cases, we have $\mathbf{R} = E\mathbf{D}$ where $E \in \mathbb{R}^{n\times q}$ is a matrix with *known* entries of 0s or 1s, indicating the state variables where nonlinear terms are absent or present, and $\mathbf{D}$ is determined accordingly. (Here, $q \le n$ denotes the number of state variables that include nonlinear terms.) It is simple to see that we can extend the analysis to this case by defining $\mathcal{D} := \{D \in \mathbb{R}^{q\times T} : DD^\top \preceq \Delta_D \Delta_D^\top\}$ where Δ_D is a design parameter, and replacing Δ_R with $E\Delta_D$ in (20) and the condition $\mathbf{R} \in \mathcal{R}$ with the condition $\mathbf{D} \in \mathcal{D}$. This modification is advantageous because it reduces the uncertainty in $\mathbf{R}$ and thus makes (20) easier to solve.

4. Case studies

To validate the effectiveness of the proposed direct data-driven control of DERs, several case studies are carried out. The DER parameters in Fig. 1 include $L_c = 2.62$ mH, $r_c = 3.5$ Ω, $vg = 380$ V, $\omega_g = 377$ rad/s. For data collection and direct control design, 50 samples were collected and the design parameter was chosen as $\Delta_R = \begin{bmatrix} 1 & 0 & 0 \\ 0 & 1 & 0 \end{bmatrix}^T$. First, performance of current regulation of the DER is tested, followed by active and reactive power tracking performance. Next case study compares the performance of the proposed direct data-driven design with conventional vector control techniques [31]. Impact of measurement noise on the performance of the proposed control design is also studied. Final case study includes real-time validation of the proposed control design using an OPAL-RT testbed. A detailed model of a DER with power electronics switching behavior is developed using MATLAB Simulink for validation of the proposed design. Parameters of the system were adopted from [32].

4.1. Current control

For current control, the controller performance was tested following the design presented in Fig. 3. The setpoints of the current controller are given by $i_d^{ref} = 15$ A and $i_q^{ref} = 10$ A. The results are shown in Fig. 4, where $\mathbf{x} = [i_{od} \ i_{oq} \ \delta]^\top$ is the state vector. For data collection and calculation of the controller gain K, historical data for 0.1 s were collected

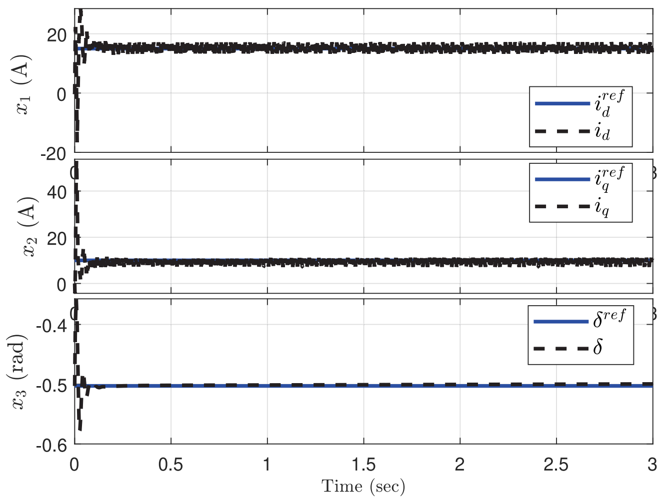

Fig. 4. Current regulation performance.

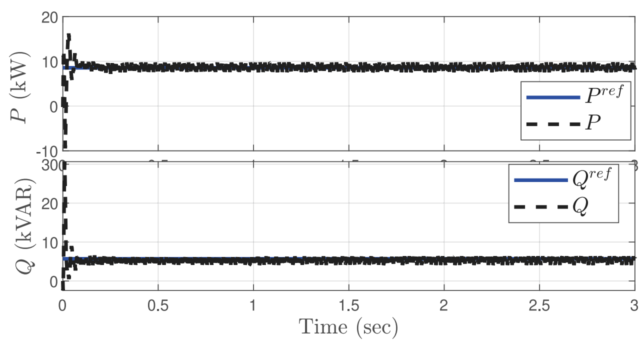

Fig. 5. Active and reactive power tracking performance.

at a sampling rate of 0.5 ms. As can be seen, the proposed data-driven control design quickly converges and can successfully provide current control tracking performance to DERs without explicit knowledge of the DER model. Such minimum data requirements can enable close to real-time implementation of the proposed control design for DERs that face model/parameter changes to adaptively update the controller gain K according to the new data collection (*i.e.*, every 0.1 s).

4.2. Active and reactive power tracking

In the second case study, the active and reactive power tracking performance of the proposed data-driven control design is evaluated. Since a phase-locked loop (PLL) is embedded in the control design that synchronizes the converter voltage with the grid voltage (see Fig. 3), $\omega_s \approx \omega_g$, and $\delta_0 \approx 0$. In this case, the active and reactive powers can be tracked according to Eq. (5). However, if $\delta_0 \neq 0$, PI regulators must be used as shown in Fig. 3. The simulation results are shown in Fig. 5, which confirm the capability of the proposed data-driven DER controller to track the active and reactive power setpoints of the DER.

4.3. Comparison with conventional vector control designs

To validate the effectiveness of the proposed control design compared with model-based approaches, a comparison is carried out, which is shown in Fig. 6. As it can be observed, the proposed approach offers faster settling time (0.2 s) compared with conventional vector controllers (1.1 s) in tracking reference currents without knowledge of the DER model and merely based on collected data. It is noted

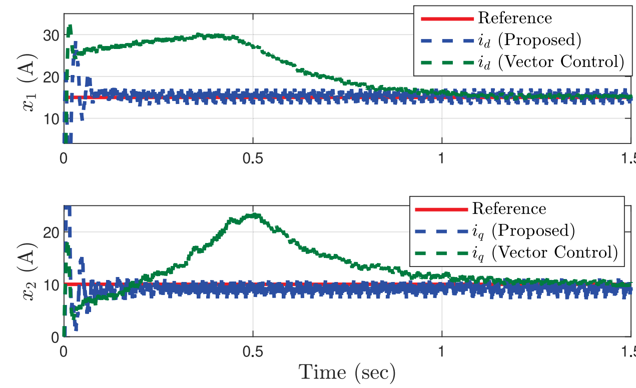

Fig. 6. Comparison with conventional vector controllers.

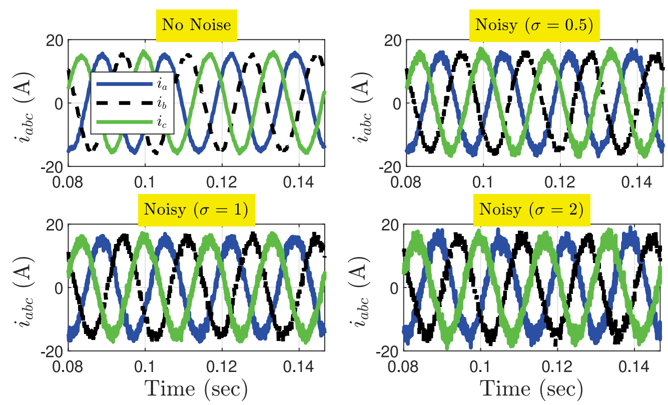

Fig. 7. Impact of Gaussian measurement noise on DER currents.

that further tuning the controller gains in conventional vector control technique will result in larger overshoots, which might exceed the maximum current limits of DC/AC converter. Therefore, the results confirm great potential for replacing current model-based DER controllers with data-driven controllers.

4.4. Robustness against measurement noise

To show the effectiveness of the proposed data-driven control against measurement noise, the state measurements $\mathbf{x} = [i_{od}\ i_{oq}\ \delta]^\top$ were injected with a noise, *i.e.*, $\tilde{\mathbf{x}} = \mathbf{x} + \mathbf{n}$, where $\tilde{\mathbf{x}}$ denotes the noisy measurement, and $\mathbf{n}$ denotes the measurement noise.

4.4.1. Gaussian noise study

In this section, $\mathbf{n} \sim \mathcal{N}(\mu, \sigma^2)$ is Gaussian measurement noise with zero mean $\mu = 0$ and standard deviation σ. We considered three different standard deviations to inject noise into current measurements of the DERs (x_1, x_2) and the results are shown in Fig. 7. The control performance under Gaussian measurement noise is shown in Fig. 8. As can be observed, measurement noise has a minimum impact on the performance of the proposed control design. Even when the standard deviation increases to 2, the control design is robust enough to ensure fast tracking and minimum transients.

4.4.2. Non-Gaussian noise study

In this section, $\mathbf{n} \sim \mathcal{U}(a, b)$ represents the uniform measurement noise with lower and upper bounds a and b, respectively. We consider three different noise levels, where the noise amplitude is set to 10%, 15% and 20% of the RMS value of the current measurements (x_1, x_2). The corresponding results are shown in Fig. 9.

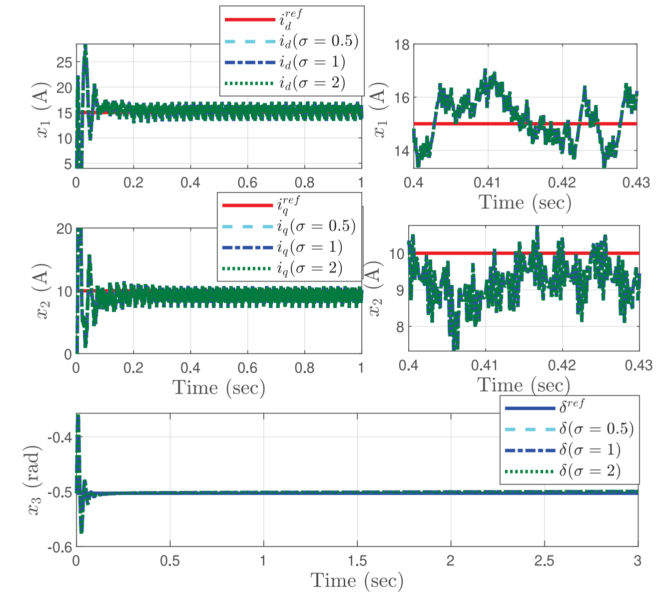

Fig. 8. Robustness of the proposed control design against Gaussian measurement noise.

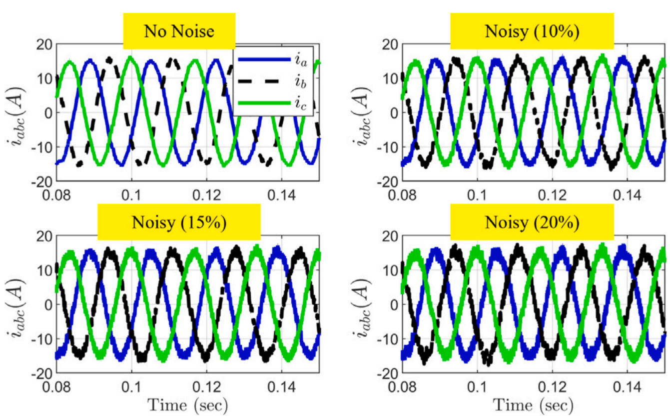

Fig. 9. Impact of Uniform measurement noise on DER currents.

The control performance under uniform measurement noise is illustrated in Fig. 10. As observed, the measurement noise has minimal impact on the performance of the proposed control design. Even at a noise level of 20% of the nominal RMS value, the controller remains robust, ensuring fast tracking and minimal transients.

4.5. Real-time simulations

The real-time setup of a microgrid shown in Fig. 11 is developed in OPAL-RT simulator as shown in Fig. 12 to verify the proposed method using real-time simulation. The simulation model of the microgrid is built in MATLAB's Simscape Power System Toolbox and compiled in RT-LAB. The model includes switched converter models with pulse width modulation (PWM) to show the effectiveness of the proposed control design on real-world converter systems. The DER system with the proposed controller on Bus 1 is modeled with a DC voltage source. The inverter is implemented using the Three-Level Bridge block in Simscape toolbox on MATLAB. The RL loads are modeled with the Three-Phase Series RLC Branch block, and the PWM is generated using the PWM Generator (3-Level) block, also in Simscape. The grid is represented by a microgrid with detailed wind turbines and battery storage modules with power electronics switching components and

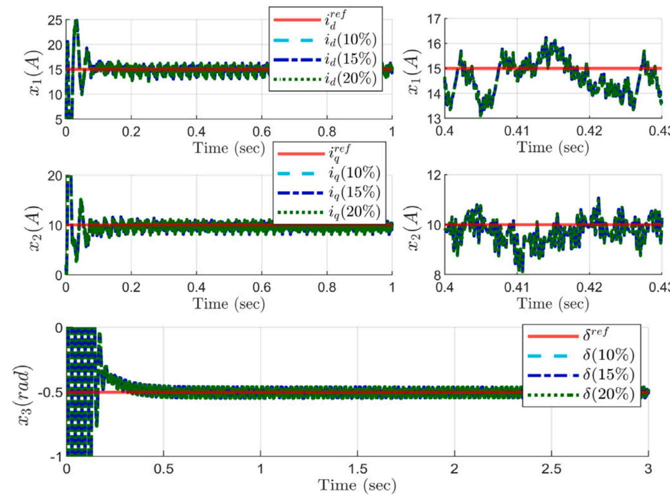

Fig. 10. Robustness of the proposed control design against Uniform measurement noise.

control design in MATLAB/Simulink). During the test, system voltages and currents are measured and fed into a phase-locked loop (PLL) to compute the dq-frame quantities. These values are then passed on to the controllers proposed in this paper to generate PWM signals that control the inverter. For the microgrid configuration, as shown in Fig. 11, the model is integrated into a three-bus microgrid to better approximate real-world conditions. Bus 1 connects to a DER with the proposed control system, Bus 2 connects to a six-generator double fed induction generator (DFIG) wind farm together with a battery energy storage system, and Bus 3 is connected to the main power grid. It should be noted that detailed models of wind turbines and a battery storage system were used to model the microgrid system. The buses are interconnected by 30 km transmission lines. The model is then loaded and executed on one of the CPU cores of the real-time target OP4510 and integrated into the Simulink® GUI running on the host PC through a TCP/IP link. Desired measurements are then sent to a digital oscilloscope in real-time via the analog outputs of the simulator.

The results of the real-time simulation for the current control performance are shown in Fig. 12. The active power set point of the DER with the proposed controller changes from $P = 3$ to 3.6 kW at 1 s and the reactive power set point changes from $Q = 2$ to 1.6 kVAR at 2 s. It is observed that the proposed control design can successfully track active and reactive power references in a real-time microgrid environment, that is close to real-world scenarios. Therefore, the proposed data-driven control design has the potential to be implemented for actual DERs in the power grid and remove the dependence of existing DER controllers on accurate dynamic models.

4.6. Benefits and limitations of real-time simulation

In this work, the control algorithm and power system models are implemented within the OPAL-RT real-time simulator. Although this setup enables the evaluation of the controller under real-time execution constraints (e.g., fixed sampling intervals and computation deadlines), it does not constitute a controller-hardware-in-the-loop (C-HIL) simulation. In true C-HIL, the controller hardware (such as a DSP or microcontroller running the control code) is physically connected to the real-time simulator via digital or analog I/Os, and generates the PWM gating signals for the simulated plant. This setup allows for an assessment of the real-world timing, computation, and interface characteristics of the controller.

Similarly, power-hardware-in-the-loop (P-HIL) extends C-HIL by interfacing with physical power hardware, such as inverters or loads.

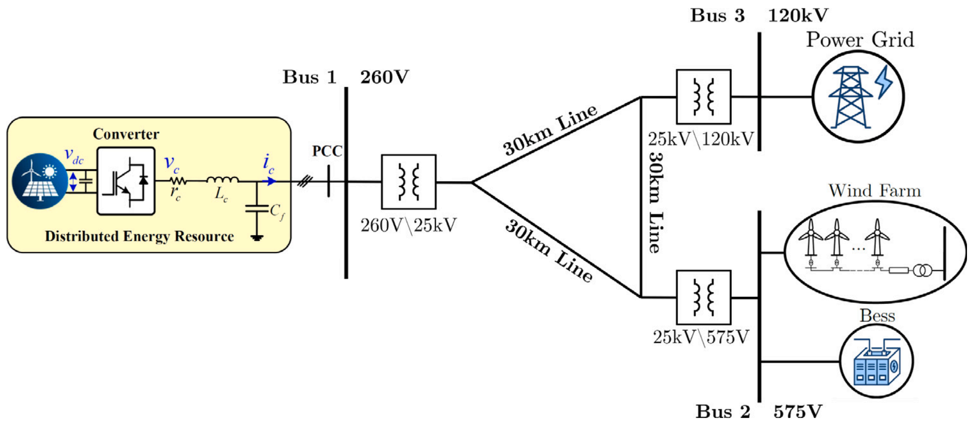

Fig. 11. Three-bus microgrid model for real-time simulation.

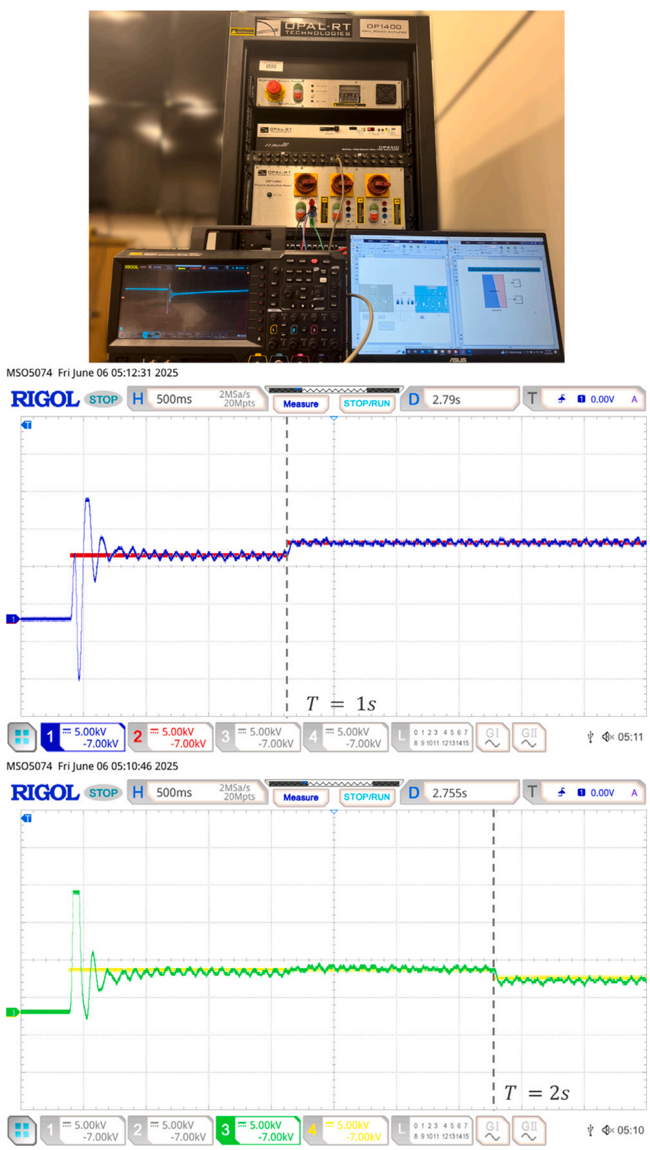

Fig. 12. Real-time simulation setup for validation of the proposed controller and P(middle) and Q(bottom) tracking performance.

Our current simulation setup should be accurately described as real-time software-in-the-loop (SIL) or real-time digital simulation, where both the control algorithm and the plant are simulated within the same platform. This approach offers significant benefits over offline simulations, including validation of control performance under strict real-time scheduling, exposure to discretization effects, and the opportunity to identify potential timing-related implementation issues. However, it does not capture all the effects of real-world hardware or interfaces (such as I/O latency, quantization, or computation delays) that may be encountered in a true C-HIL or P-HIL environment.

5. Conclusions

In this paper, we present a novel model-free approach for controlling distributed energy resource systems. This approach directly utilizes data as a non-parametric model of the system, thereby bypassing any identification steps. Compared to classical model-based methods, this approach is therefore more straightforward from a practical standpoint, yet it demonstrates favorable performance, as highlighted in the simulation results and experimental tests. Furthermore, the method offers several advantages over emerging design methods based on machine learning techniques, including efficient data utilization, interpretability, and the ability to provide stability guarantees for the control system.

An interesting direction for future research involves the development of control systems that, in addition to stability, ensure *contractivity* [33]. Contractivity does not necessitate explicit knowledge of the equilibrium point, as is required in this approach. However, the results in [33] only consider state-independent input vector fields and therefore must be extended to accommodate the setting discussed in this paper.

CRediT authorship contribution statement

Zhongtian Zhang: Validation. **Javad Khazaei:** Writing – review & editing, Writing – original draft. **Faegheh Moazeni:** Writing – review & editing, Writing – original draft. **Pietro Tesi:** Writing – review & editing, Writing – original draft. **Claudio De Persis:** Writing – review & editing, Writing – original draft.

Declaration of competing interest

The authors declare the following financial interests/personal relationships which may be considered as potential competing interests: Javad Khazaei reports financial support was provided by National Science Foundation under Grant NSF-EPCN 2221784. If there are other authors, they declare that they have no known competing financial interests or personal relationships that could have appeared to influence the work reported in this paper.

Data availability

Data will be made available on request.

References

[1] Joint NERC and WECC staff report. San fernando disturbance, south california event, 2020, https://www.nerc.com/pa/rrm/ea/Documents. (Accessed 30 December 2021).

[2] A. Yazdani, R. Iravani, Voltage-Sourced Converters in Power Systems: Modeling, Control, and Applications, John Wiley & Sons, 2010.

[3] S.B. Siad, A. Malkawi, G. Damm, L. Lopes, L.G. Dol, Nonlinear control of a DC MicroGrid for the integration of distributed generation based on different time scales, Int. J. Electr. Power Energy Syst. 111 (2019) 93–100.

[4] Y. Toghani Holari, S.A. Taher, M. Mehrasa, Distributed energy storage system-based nonlinear control strategy for hybrid microgrid power management included wind/PV units in grid-connected operation, Int. Trans. Electr. Energy Syst. 30 (2) (2020) e12237.

[5] Y. Mchaouar, A. Abouloifa, A. Elallali, C. Taghzaoui, I. Lachkar, J.M. Guerrero, Advanced sensorless nonlinear control strategy for grid connected photovoltaic systems via the two-time scale singular perturbation technique, Int. J. Power Electron. 17 (2) (2023) 129–165.

[6] S. Sabzevari, R. Heydari, M. Mohiti, M. Savaghebi, J. Rodriguez, Model-free neural network-based predictive control for robust operation of power converters, Energies 14 (8) (2021) 2325.

[7] X. Shi, Y. Cao, M. Shahidehpour, Y. Li, X. Wu, Z. Li, Data-driven wide-area model-free adaptive damping control with communication delays for wind farm, IEEE Trans. Smart Grid 11 (6) (2020) 5062–5071.

[8] M. Khalilzadeh, S. Vaez-Zadeh, J. Rodriguez, R. Heydari, Model-free predictive control of motor drives and power converters: A review, Ieee Access 9 (2021) 105733–105747.

[9] D. Cao, W. Hu, J. Zhao, G. Zhang, B. Zhang, Z. Liu, Z. Chen, F. Blaabjerg, Reinforcement learning and its applications in modern power and energy systems: A review, J. Mod. Power Syst. Clean Energy 8 (6) (2020) 1029–1042.

[10] Y. Cheng, L. Fan, Wind Energy Systems Sub-Synchronous Oscillations: Events and Modeling, IEEE Power & Energy Society: Piscataway, NJ, USA, 2020.

[11] J. Shair, X. Xie, L. Wang, W. Liu, J. He, H. Liu, Overview of emerging subsynchronous oscillations in practical wind power systems, Renew. Sustain. Energy Rev. 99 (2019) 159–168.

[12] M.V. Kazemi, S.J. Sadati, S.A. Gholamian, Adaptive frequency control of microgrid based on fractional order control and a data-driven control with stability analysis, IEEE Trans. Smart Grid 13 (1) (2022) 381–392.

[13] M. Zhang, Z. Miao, L. Fan, S. Shah, Data-driven interarea oscillation analysis for a 100% IBR-penetrated power grid, IEEE Open Access J. Power Energy 10 (2023) 93–103.

[14] S. Formentin, A. Chiuso, Control-oriented regularization for linear system identification, Automatica 127, 109539 (2021).

[15] Z. Hu, C. De Persis, P. Tesi, Learning controllers from data via kernel-based interpolation, in: 62nd IEEE Conference on Decision and Control, CDC, IEEE, 2023, pp. 8509–8514.

[16] M. Khalilzadeh, S. Vaez-Zadeh, J. Rodriguez, R. Heydari, Model-free predictive control of motor drives and power converters: A review, Ieee Access 9 (2021) 105733–105747.

[17] Y. Chen, Y. Lin, Combining model-based and model-free methods for stochastic control of distributed energy resources, Appl. Energy 283 (2021) 116204.

[18] C. De Persis, P. Tesi, Formulas for data-driven control: Stabilization, optimality, and robustness, IEEE Trans. Autom. Control 65 (3) (2020) 909–924.

[19] C. De Persis, P. Tesi, Learning controllers for nonlinear systems from data, Annu. Rev. Control. (2023) 100915.

[20] R. Pérez-Ibacache, C.A. Silva, A. Yazdani, Linear state-feedback primary control for enhanced dynamic response of AC microgrids, IEEE Trans. Smart Grid 10 (3) (2018) 3149–3161.

[21] A. Yazdani, R. Iravani, Voltage-Sourced Converters in Power Systems: Modeling, Control, and Applications, John Wiley & Sons, 2010.

[22] X. Dai, C. De Persis, N. Monshizadeh, P. Tesi, Data-driven control of nonlinear systems from input-output data, in: 62nd IEEE Conference on Decision and Control, CDC, IEEE, 2023, pp. 1613–1618.

[23] H.K. Khalil, Nonlinear Control Systems, third ed., Prentice Hall Upper Saddle River, NJ, 2002.

[24] C. Scherer, S. Weiland, Linear matrix inequalities in control, in: Lecture Notes, vol. 3, (2) Dutch Institute for Systems and Control, Delft, he Netherlands, 2000.

[25] S. Larsson, V. Thomée, Partial differential equations with numerical methods, vol. 45, Springer, 2003.

[26] J. Khazaei, W. Liu, F. Moazeni, Data-driven sparse model identification of inverter-based resources for control in smart grids, in: 2023 11th International Conference on Smart Grid (IcSmartGrid), IEEE, 2023, pp. 1–6.

[27] C. De Persis, P. Tesi, Learning controllers for nonlinear systems from data, Annu. Rev. Control. 100915 (2023).

[28] M. Guo, C. De Persis, P. Tesi, Data-driven stabilization of nonlinear polynomial systems with noisy data, IEEE Trans. Autom. Control 67 (8) (2022) 4210–4217.

[29] M. Alsalti, V. Lopez, M. Müller, On the design of persistently exciting inputs for data-driven control of linear and nonlinear systems, IEEE Control. Syst. Lett. 66 (2023) 2629–2634.

[30] J. Khazaei, A. Hosseinipour, Data-driven feedback linearization control of distributed energy resources using sparse regression, IEEE Trans. Smart Grid 15 (2) (2023) 2282–2293.

[31] Q. Liu, T. Caldognetto, S. Buso, Review and comparison of grid-tied inverter controllers in microgrids, IEEE Trans. Power Electron. 35 (7) (2019) 7624–7639.

[32] J. Khazaei, Z. Tu, A. Asrari, W. Liu, Feedback linearization control of converters with LCL filter for weak AC grid integration, IEEE Trans. Power Syst. 36 (4) (2021) 3740–3750.

[33] Z. Hu, C. De Persis, P. Tesi, Enforcing contraction via data, 2024, arXiv:2401.07819.